

Investigating the possibility of locating microseismic sources using distributed sensor networks^a

^aPublished in SEG Expanded Abstracts, 2485-2490, (2015)

*Junzhe Sun, Tieyuan Zhu, Sergey Fomel, The University of Texas at Austin, and
Wen-Zhan Song, Georgia State University*

ABSTRACT

Distributed sensor networks are designed to provide computation in-situ and in real-time. The conventional time-reversal imaging approach for microseismic event location may not be optimal for such an environment. To address this challenge, we develop a methodology of locating multiple microseismic events with unknown start times based on the cross-correlation imaging condition borrowed from active-source seismic imaging. The imaging principle states that a true microseismic source must correspond to the location where all the backward-propagated events coincide in both space and time. Instead of simply stacking the backward-propagated seismic wavefields, as suggested by time-reversal imaging, we perform multiplication reduction to compute a high-resolution microseismicity map. The map has an extra dimension of time, indicating the start times of different events. Combined with a distributed sensor network, our method is designed for monitoring microseismic activities and mapping fracture development during hydraulic fracturing in-situ and in real-time. We use numerical examples to test the ability of the proposed technique to produce high-resolution images of microseismic locations.

INTRODUCTION

The development of unconventional reservoirs relies on hydraulic fracturing, a technique that stimulates fracture network and enhances permeability by injecting high-pressure fluids into production formations (Montgomery and Smith, 2010). Microseismic monitoring is currently the only technique that can provide real-time information about the geometry of stimulated fracture network (Maxwell, 2014). The key task in microseismic monitoring is locating microseismic events. The traditional method for microseismic imaging is arrival-time inversion with traveltimes picked adopted from earthquake seismology (Gibowicz and Kijko, 2013). However, the microseismic data often contain unidentifiable P or S-wave signals emerging from strong background noise, e.g., surface microseismic data (Duncan and Eisner, 2010). This makes travel-time picking challenging.

Recently progress has been made in locating seismic sources with minimum or without traveltimes picking. Rentsch et al. (2006) and Rentsch et al. (2010) developed a source location method inspired by Gaussian-beam migration, which has low sensitivity to picking precision. Kao and Shan (2004) introduced a source-scanning algorithm in which data are aligned and stacked based on the traveltimes from speculative image points in a manner similar to diffraction-stack (Kirchhoff) migration. Instead of using traveltimes, Gajewski and Tessmer (2005) back propagated full-waveform data by reverse-time modeling (McMechan, 1982). Artman et al. (2010) and Witten and Artman (2011) generalized this approach using P- and S-waves. Zhu (2014) improved the source properties by applying attenuation compensation. Time-reversal imaging is capable of inferring both the location and the start time of a point source, however, it may fail to locate rupture propagation (Kremers et al., 2011), i.e., multiple sources clustered along the time axis. Detecting and discerning each hypocenter therefore requires an evolving microseismic image that has high-resolution in both space and time.

Distributed sensor networks are designed to perform computation in-situ and in real-time. Recently, they have been used for seismic tomography based on the advanced wireless sensor network technology and distributed computing algorithms (Shi et al., 2013; Song et al., 2015). Instead of collecting data to a central place for processing, the distributed seismic data processing and computing can be performed on a single sensor or locally on a few sensors. The results are then gathered for real-time visualization. Employing distributed sensor networks for microseismic monitoring requires a distributed microseismic location algorithm.

In this paper, we develop a distributed microseismic imaging algorithm that is inspired by both passive-source time-reversal imaging and active-source migration imaging. The key innovation is that the imaging principle requires that the imaged hypocenters must correspond to locations where all the wavefields individually backward-propagated from each receiver coincide in both space and time. Our method should be capable of producing high-resolution images of multiple source locations, even when the signal-to-noise ratio (SNR) is low. The processing framework detailed in this paper is naturally suited for distributed sensor networks.

We first introduce the cross-correlation imaging condition for locating microseismic sources and establish a connection with time-reversal imaging. Synthetic examples are used to test the ability of the proposed approach to image multiple microseismic locations at once. We discuss a possible application of the proposed framework to real-time in-situ microseismic monitoring on distributed sensor networks.

THEORY

In prestack seismic reflection imaging, a reflector is imaged when the source wavefield coincides with the receiver wavefield in both space and time (Claerbout, 1985). For poststack or zero-offset data, reflectors can be imaged using the exploding reflector

concept (Loewenthal et al., 1976). The imaging condition of exploding reflector is similar to that of time-reversal imaging, which states that the backward-propagated wavefield at zero time corresponds to the reflectors/sources. The principle of time-reversal imaging can be used for locating passive earthquake hypocenters (Gajewski and Tessmer, 2005). All the aforementioned imaging conditions require the start times of seismic sources to be available, which is not the case for microseismic data. Therefore, most existing time-reversal imaging algorithms need to perform scanning and picking on a group of potential start times (Fink, 2006; Maxwell, 2014).

Motivated by the development of distributed sensor networks, we propose to adopt the imaging principle of prestack migration for locating microseismic hypocenters. We treat the wavefield back propagated from each individual receiver as an independent wavefield, and define microseismic hypocenters as the locations where all the wavefields coincide in both space and time. The imaging condition is formulated as a multiplication reduction of all the back propagated wavefields, calculated using data from each receiver:

$$I(\mathbf{x}, t) = \prod_{i=0}^{N-1} R_i(\mathbf{x}, t) . \quad (1)$$

A similar technique was developed by Nakata (2015, personal communication). Assuming the velocity model is accurate and data contains zero noise, the image $I(\mathbf{x}, t)$ should have non-zero values only if all the backward-propagated wavefields are non-zero at location \mathbf{x} and time t , i.e., the starting of an earthquake. When noise is present in the data, extra non-zero values might appear in the image. However, as long as the noise has certain randomness, the amplitude of these false image points will be much weaker than those generated by coherent signal, and thresholding can effectively separate the non-zero values result from noise. The image $I(\mathbf{x}, t)$ calculated by equation 1 therefore indicates the seismicity at time t . The resolution of the image depends on the frequency content of the wavefields.

The conventional time-reversal imaging can be formulated in a similar fashion. Instead of performing multiplication, the image is produced by summing over all the receiver wavefields:

$$I(\mathbf{x}, t) = \sum_{i=0}^{N-1} R_i(\mathbf{x}, t) . \quad (2)$$

In practice, this is done by backward-propagating all the data at once and the summation is implicit. When applied to microseismic data from multiple sources, it is usually a challenging task to pick the hypocenters from the complicated wavefield, especially when the data has a low SNR.

The cross-correlation imaging condition (equation 1) and time-reversal imaging condition (equation 2) represent two extremes. The image produced by equation 1 is high-resolution and easy to pick, since only non-zero values in the image correspond to hypocenters. However, it requires propagating the wavefields using data from each receiver separately, and thus is computationally intensive. Equation 2, on the other hand, requires essentially only one computation using the entire data set, but has

less resolving power and is less suitable for distributed networks. A hybrid imaging condition would combine the merits of the two:

$$I(\mathbf{x}, t) = \prod_{j=0}^{N/n-1} \sum_{k=0}^{n-1} R_{j \times n+k}(\mathbf{x}, t), \quad (3)$$

where n is the local summation window length. Length n should be selected such that neighboring receivers are backward-propagated together while far-apart receivers are cross-correlated. Equation 3 requires N/n computations of reverse-time modeling. In principle, both equation 1 and 3 need to perform cross-correlation using at least three wavefields to constrain one point in space. Schematically, the differences between the three imaging conditions is shown in Figure 1.

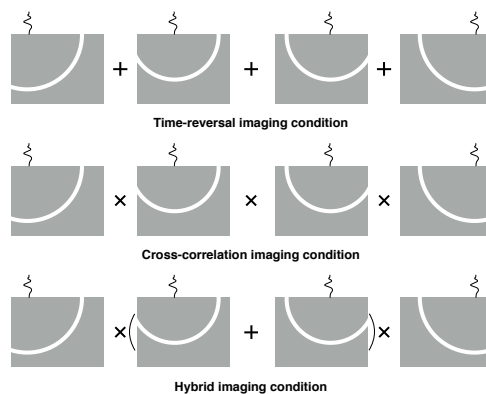


Figure 1: Different imaging conditions for locating microseismic sources. A homogeneous medium and four receiver stations are assumed. A hybrid imaging condition calculates local summation before applying cross-correlation. In practice, the summation is performed implicitly by back propagating data from several neighboring receivers at once.

A movie of accumulated seismicity can be generated by performing an integration over time:

$$M(\mathbf{x}, t) = \int_0^t I(\mathbf{x}, \tau) d\tau, \quad (4)$$

Movie $M(\mathbf{x}, t)$ is an evolving map of microseismicity in time that could be used to indicate rupture propagation. An image of all the sources corresponds the last instance of $M(\mathbf{x}, t)$.

NUMERICAL EXAMPLES

In the following examples we demonstrate the performance of the proposed method using two synthetic data experiments. We employ the pseudo-spectral method (Reshef et al., 1988) to solve the acoustic wave equation, with an exponential decay absorbing boundary condition (Cerjan et al., 1985). The seismic sources are assumed to be a

Ricker wavelet with a peak frequency of 20 Hz . The examples involve a number of simplifications but are designed simply to test the concept of microseismic imaging by cross-correlation imaging condition.

Three-layer model

In the first example, we used a three-layer model with six assumed microseismic sources located within the middle layer (Figure 2a). The model is discretized on a 140×140 grid with 15 m spacing in both vertical and horizontal directions. The model has sharp velocity contrasts, which generate multiple reflection events in both forward and backward propagation.

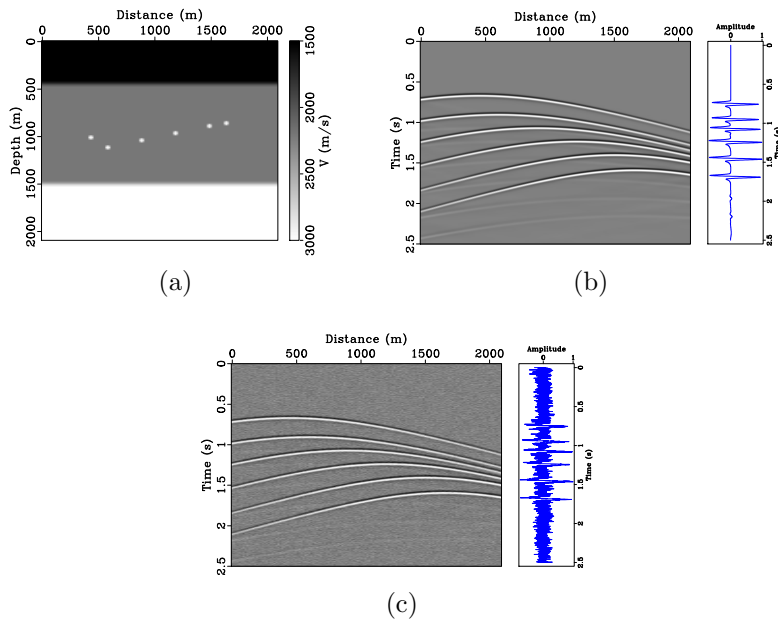


Figure 2: (a) Microseismic source locations overlaid on a three-layer velocity model. (b) Noise-Free microseismic data from three-layer model. (c) Noisy microseismic data from three-layer model. The traces displayed in the right panel correspond to $X = 1050 m$. [cross/sov1,datatrace-clean,datatrace-noisy](#)

We first use noise-free data (Figure 2b) to test the sensitivity of the cross-correlation imaging condition to stratigraphic boundaries, which are common in unconventional reservoirs. We use data from only 10 surface stations starting from $X = 75 m$ and ending at $X = 1965 m$, with an interval of 210 m . After individually backward-propagating the receiver wavefields and applying the cross-correlation imaging condition (equation 1), we obtain a clean, high-resolution image which accurately locates all the correct hypocenters (Figure 3a).

Next we introduce a strong random noise into the data (Figure 3b) to test the sensitivity of the method in such a setting. By keeping the number of receivers un-

changed, the final image contains some false image points clustered around reflection boundaries. Additionally, although the image still contains all the true hypocenters, they are not well focused, i.e., some of the true hypocenters split across neighboring points.

To remove the artifacts caused by a low SNR, we employ the hybrid imaging condition (equation 3) by including five receivers in one station. For example, the station at $X = 75 \text{ m}$ now includes five receivers with an interval of 15 m . We still perform ten backward propagations, with each wavefield using data from five neighboring receivers. The image contains significantly less artifacts, with only one defocused point corresponding to the rightmost hypocenter (Figure 3c).

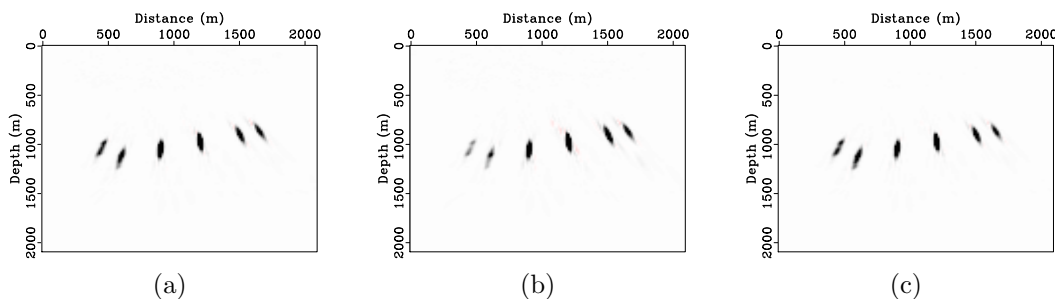


Figure 3: (a) Microseismic source locations imaged by the cross-correlation imaging condition using noise-free data. (b) Microseismic source locations imaged by the cross-correlation imaging condition using noisy data. (c) Microseismic source locations imaged by the hybrid imaging condition using noisy data.

[cross/ location0-clean,location0-noisy,location0-hyb](#)

Marmousi model

For the second example, we create a somewhat more realistic scenario by using a portion of the Marmousi velocity model (Versteeg, 1994). The model dimension is 200×200 with a spatial sampling rate of 8 m along the vertical direction and 12 m along the horizontal direction. The model features a series of nearly parallel stratigraphic layers. To mimic an imaginary hydraulic fracturing process, we design three periods of assumed microseismicity propagating from left to right with a total of eighteen hypocenters, which corresponds to three stages of perforations (Figure 4). The data has a high level of random background noise (Figure 5). We employ the hybrid imaging condition using ten stations starting from $X = 0 \text{ m}$ with a spacing of 240 m . Each station is again comprised of five neighboring sensors with an interval of 12 m . The images computed from the surface array data accurately locates all the hypocenters, and evolve with time according to equation 4 (Figures 6a, 6b and 6c).

So far we have been focusing on using data from surface arrays. Recently, there is a growing use of multiple monitoring configurations such as combining downhole

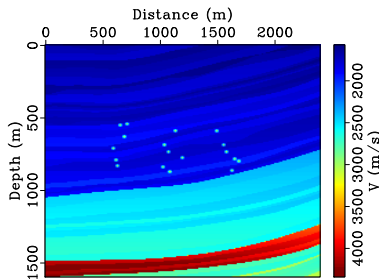


Figure 4: Microseismic source locations overlaid on Marmousi velocity model. A total of three stages of microseismicity are assumed, each with six hypocenters. [marm/sov](#)

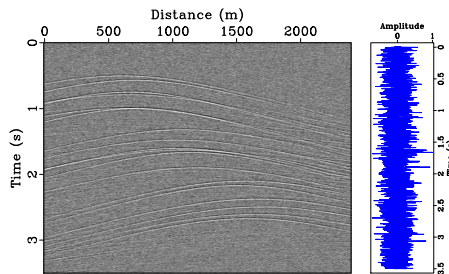


Figure 5: Noisy microseismic data from Marmousi model. The trace in the right panel corresponds to $X = 1.2 \text{ km}$. [marm/datatrace](#)

arrays with surface sensors to provide better wavefield sampling (Maxwell, 2014). If available, data from downhole arrays/sensors can actually help improve the spatial resolution of imaged source locations, particularly in the vertical direction. In the last test, we combine data from the original surface arrays with data from four extra downhole sensors located at $X = 0 \text{ km}$ and $Z = [0.24 \text{ km}, 0.64 \text{ km}, 1.04 \text{ km}, 1.44 \text{ km}]$ respectively. The corresponding images demonstrate significantly higher vertical resolution thanks to the better sampling of the wavefield (Figures 6d, 6e and 6f). Our experiment confirms that combining surface and vertical borehole arrays can improve image resolution.

DISCUSSION AND CONCLUSIONS

Real-time microseismic monitoring provides invaluable information about stimulated fracture networks during hydraulic fracturing. Recently, wireless sensor networks have emerged as an effective tool for surface monitoring (Song et al., 2009). Wireless networks are easier to deploy than wired networks. Additionally, the computation and communication capabilities of sensor nodes can be utilized for in-situ data processing in real-time (Kamath et al., 2013; Song et al., 2015). To enable microseismic monitoring using computation on distributed sensor networks, we have presented an approach where wavefield propagation can be performed independently using data collected by each station. Future research involves optimizing image reduction un-

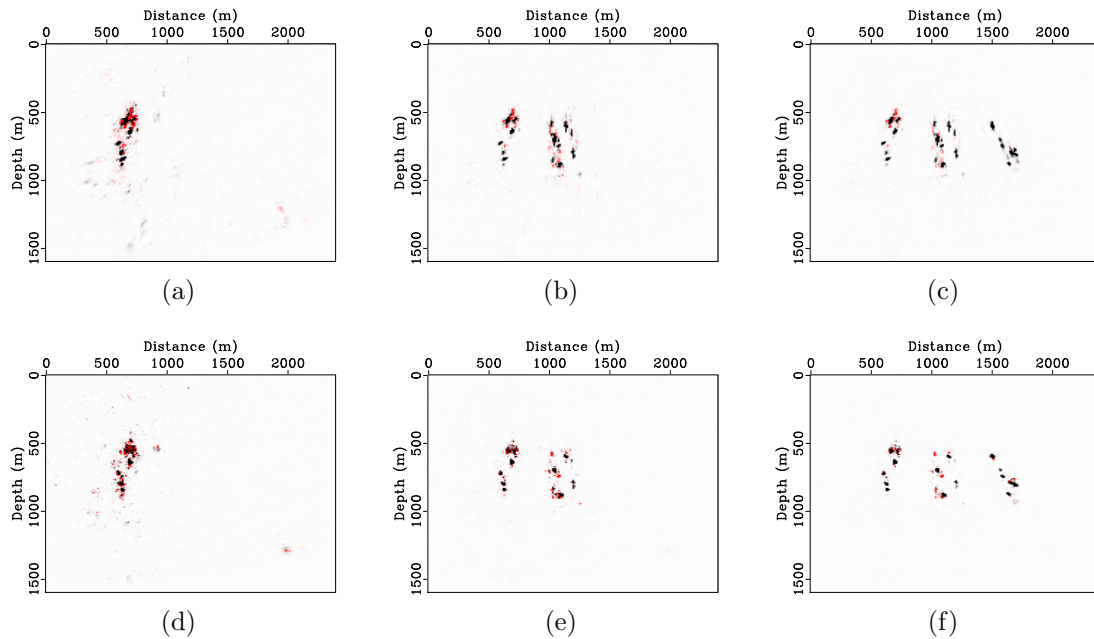


Figure 6: Accumulated microseismicity calculated by the hybrid imaging condition using: (a)-(c) noisy data from surface array; (d)-(f) noisy data from both surface array and downhole sensors. Each column is produced after one stage of perforation.

[marm/ stage0-1,stage0-2,stage0-3,stage-1,stage-2,stage-3](#)

der the constraint of the wireless network resources (bandwidth, energy, computing power, memory, etc).

A cross-correlation imaging condition for locating microseismic hypocenters is capable of producing high-resolution images in both space and time, and is robust with respect to noise when used in a hybrid formulation. Combined with a distributed sensor network, the proposed technique should be able to provide real-time in-situ microseismic monitoring of stimulated fracture network during hydraulic fracturing.

ACKNOWLEDGMENTS

We thank Nori Nakata and Yangkang Chen for helpful discussions. We thank TCCS sponsors for financial support. The first author is supported additionally by the Statoil Fellows Program at UT Austin. The second author is supported by the Jackson School Distinguished Postdoctoral Fellowship at UT Austin. The fourth author acknowledges the support of the JTO faculty fellowship in the ICES at UT Austin.

REFERENCES

- Artman, B., I. Podladtchikov, and B. Witten, 2010, Source location using time-reverse imaging: *Geophysical Prospecting*, **58**, 861–873; doi: 10.1111/j.1365-2478.2010.00911.x.
- Cerjan, C., D. Kosloff, R. Kosloff, and M. Reshef, 1985, A nonreflecting boundary condition for discrete acoustic and elastic wave equations: *Geophysics*, **50**, 705–708.
- Claerbout, J. F., 1985, *Imaging the Earth’s interior*: Blackwell Scientific Publications.
- Duncan, P. M., and L. Eisner, 2010, Reservoir characterization using surface microseismic monitoring: *Geophysics*, **75**, 75A139–75A146; doi: 10.1190/1.3467760.
- Fink, M., 2006, Time-reversal acoustics in complex environments: *Geophysics*, **71**, SI151–SI164.
- Gajewski, D., and E. Tessmer, 2005, Reverse modelling for seismic event characterization: *Geophysical Journal International*, **163**, 276–284; doi: 10.1111/j.1365-246X.2005.02732.x.
- Gibowicz, S. J. ., and A. Kijko, 2013, *An introduction to mining seismology*: Elsevier.
- Kamath, G., L. Shi, and W.-Z. Song, 2013, Component-average based distributed seismic tomography in sensor networks: Presented at the The 9th IEEE International Conference on Distributed Computing in Sensor Systems (IEEE DCOSS).
- Kao, H., and S.-J. Shan, 2004, The source-scanning algorithm: mapping the distribution of seismic sources in time and space: *Geophysical Journal International*, **157**, 589–594; doi: 10.1111/j.1365-246X.2004.02276.x.
- Kremers, S., A. Fichtner, G. B. Brietzke, H. Igel, C. Larmat, L. Huang, and M. Käser, 2011, Exploring the potentials and limitations of the time-reversal imaging of finite seismic sources: *Solid Earth*, **2**, 95–105; doi: 10.5194/se-2-95-2011.
- Loewenthal, D., L. Lu, R. Roberson, and J. Sherwood, 1976, The wave equation applied to migration: *Geophysical Prospecting*, **24**, 380–399.
- Maxwell, S., 2014, *Microseismic imaging of hydraulic fracturing: Improved engineering of unconventional shale reservoirs*: SEG.
- McMechan, G. A., 1982, Determination of source parameters by wavefield extrapolation: *Geophysical Journal of the Royal Astronomical Society*, **71**, 613–628; doi: 10.1111/j.1365-246X.1982.tb02788.x.
- Montgomery, C. T., and M. B. Smith, 2010, Hydraulic fracturing: A history of an enduring technology: *Journal of Petroleum Technology*, **62**, 26–32.
- Rentsch, S., S. Buske, S. Gutjahr, J. Kummerow, and S. Shapiro, 2010, Migration-based location of seismicity recorded with an array installed in the main hole of the San Andreas Fault Observatory at Depth (SAFOD): *Geophysical Journal International*, **182**, 477–492.
- Rentsch, S., S. Buske, S. Lüth, and S. Shapiro, 2006, Fast location of seismicity: A migration-type approach with application to hydraulic-fracturing data: *Geophysics*, **72**, S33–S40.
- Reshef, M., D. Kosloff, M. Edwards, and C. Hsiung, 1988, Three-dimensional acoustic modeling by the Fourier method: *Geophysics*, **53**, 1175–1183.
- Shi, L., W.-Z. Song, M. Xu, Q. Xiao, J. M. Lee, and G. Xing, 2013, *Imaging Seismic Tomography in Sensor Network*: Presented at the IEEE SECON.

- Song, W., L. Shi, and G. Kamath, 2015, Real-time in-situ seismic imaging: Overview and case study: 85th Annual International Meeting, SEG, Expanded Abstracts, submitted.
- Song, W.-Z., R. Huang, M. Xu, A. Ma, B. Shirazi, and R. Lahusen, 2009, Air-dropped Sensor Network for Real-time High-fidelity Volcano Monitoring: Presented at the 7th Annual International Conference on Mobile Systems, Applications and Services (MobiSys).
- Versteeg, R., 1994, The Marmousi experience: Velocity model determination on a synthetic complex data set: *The Leading Edge*, **13**, 927–936.
- Witten, B., and B. Artman, 2011, Signal-to-noise estimates of time-reverse images: *Geophysics*, **76**, MA1–MA10; doi: 10.1190/1.3543570.
- Zhu, T., 2014, Time-reverse modelling of acoustic wave propagation in attenuating media: *Geophysical Journal International*, **197**, 483–494.